Beyond FT-IR Spectroscopy: EC-QCL based mid-IR Transmission Spectroscopy of Proteins in the Amide I and Amide II Region

Andreas Schwaighofer,[†,‡] Milagros Montemurro,[†,§,‡] Stephan Freitag,[†] Christian Kristament,[†] María J. Culzoni,[§] Bernhard Lendl[*,†]

[†]Institute of Chemical Technologies and Analytics, Vienna University of Technology, Getreidemarkt 9/164-UPA, 1060 Vienna, Austria

[§]Laboratorio de Desarrollo Analítico y Quimiometría (LADAQ), Cátedra de Química Analítica I, Facultad de Bioquímica y Ciencias Biológicas, Universidad Nacional del Litoral-CONICET, Ciudad Universitaria, 3000 Santa Fe, Argentina

ABSTRACT: In this work, we present a setup for mid-IR measurements of the protein amide I and amide II bands in aqueous solution. Employing a latest generation external cavity-quantum cascade laser (EC-QCL) at room temperature in pulsed operation mode allowed implementing a high optical path length of 31 μm that ensures robust sample handling. By application of a data processing routine, which removes occasionally deviating EC-QCL scans, the noise level could be lowered by a factor of 4. The thereby accomplished signal-to-noise ratio is better by a factor of approx. 2 compared to research-grade FT-IR spectrometers at equal acquisition times. Employing this setup, characteristic spectral features of three representative proteins with different secondary structures could be measured at concentrations as low as 1 mg mL^{-1}. Mathematical evaluation of the spectral overlap confirms excellent agreement of the QCL-IR transmission measurements with protein spectra acquired by FT-IR spectroscopy. The presented setup combines performance surpassing FT-IR spectroscopy with large applicable optical paths and coverage of the relevant spectral range for protein analysis. This holds high potential for future EC-QCL based protein studies, including the investigation of dynamic secondary structure changes and chemometrics-based protein quantification in complex matrices.

Fourier transform infrared (FT-IR) spectroscopy is a well-established and powerful technique for analysis of the structure and dynamics of polypeptides and proteins.[1-3] Vibrations of the polypeptide repeat units of proteins result in nine characteristic group frequencies in the mid-IR region referred to as amide bands. The differing pattern of hydrogen bonding, dipole–dipole interactions and geometric orientations in the α-helices, β-sheets, turns and random coil structures induce different frequencies of the C=O and N-H vibrations that can be correlated with the respective secondary structural folding.[4] The amide I band (1700–1600 cm^{-1}) originating from the C=O stretching and N-H in-phase bending vibration of the amide group has been recognised to be most sensitive to secondary structure.[5,6] Furthermore, also the amide II band (1600–1500 cm^{-1}) arising from N–H bending and C–N stretching vibrations was shown to be sensitive to protein structure.[7] It has been shown that additional and more in-depth information about protein secondary structure can be gained by collective analysis of both spectral regions, particularly with chemometric analysis.[8-10]

IR transmission measurements are frequently employed for studies of protein structure in solution. A limitation when working with proteins in aqueous solution is the strong absorbance of the HOH bending vibration of water centered at 1645 cm^{-1}, that overlaps with the protein amide I band. Thus, applicable path lengths are restricted to <10 μm to prevent total IR absorption in this region.[11] Consequently, high protein concentrations (>10 mg mL^{-1}) are required, as these low path lengths limit the intensities of the IR bands and the signal-to-noise ratio (SNR) at a given concentration.[5] Furthermore, experimental challenges in cell and sample handling arise due to the low flow cross section that lead to a large pressure drop in the cell and vulnerability to cell clogging.

More than two decades ago, first quantum cascade lasers (QCLs) were introduced as a new light source for the mid-IR region that provide polarized and coherent light with spectral power densities several orders of magnitude higher than thermal light.[12] They are unipolar lasers based on intersubband transitions of electrons within the semiconductors conduction band. Due to the limited tuning range of only a few wavenumbers, distributed feedback (DFB) lasers were predominantly employed for gas phase analysis.[13] Ten years ago, a new type of these mid-IR lasers, external-cavity QCL (EC-QCLs) became commercially available, which combine high emission powers with spectral tuning ranges of several hundred wavenumbers. The high available emission powers enabled to employ 4-5 times larger path lengths for transmission measurements of glucose[14-16] and proteins[17-22] than achievable with conventional FT-IR spectrometers.

Furthermore, EC-QCLs were employed for broadband IR transmission measurements to study protein dynamics by fast kinetic experiments at high temporal resolution.[23-25] IR measurements of diverse liquid samples were performed using waveguides[26,27] and the ATR[28] technique. In addition, a method was presented for indirect absorbance detection in the form of an EC-QCL based photothermal phase shift interferometer.[29] Apart from absorption measurements, the polarized nature of the emitted light was utilized for vibrational circular dischroism (VCD) measurements.[30-32] Further, the coherence of the emitted QCL light enabled to develop a Mach–Zehnder interferometer to simultaneously record absorption and dispersion spectra of liquid samples.[33]

These manifold examples demonstrate that the unique properties of EC-QCLs led to the implementation of novel experimental approaches and applications in different fields.[34] However so far, their basic advantage of the provided high emission power could not effectively be translated to significantly higher signal-to-noise ratios than in FT-IR spectroscopy in the case of broadband transmission spectroscopy. FT-IR spectroscopy is currently considered as the gold standard due to its broad spectral range covering the entire mid-IR region, excellent SNR and, finally, the absolute wavenumber accuracy, originating from the precise interferometer control by the HeNe laser interferogram. This wavenumber accuracy facilitates scan averaging in order to achieve the notoriously low noise levels. In FT-IR spectroscopy, the final signal noise is determined by the detector noise, due to the low noise levels of the low power thermal light sources. The detected signal contains both the optical signal and the noise, which has its own frequency spectrum, and consequently the noise power is distributed over the complete spectral range by the Fourier transformation.[35]

A pronounced drawback for 1st generation EC-QCL light sources are the mechanical imperfections of the external cavity. Triggering inaccuracies and imprecisions throughout the motion of the grating introduce a constant and variable spectral mismatch in the fine structure of consecutive scans in the time (i.e. wavenumber) axis of the emitted spectrum. This small deviation of only approx. 0.5 cm^{-1} in the single beam spectrum (i) prevents efficient scan averaging for noise reduction and (ii) introduces significant noise in the corresponding absorbance spectrum. Consequently, processing routines of the measured raw data were implemented to reduce the effects of this spectral mismatch. Initially, shifting of the recorded scans along the time axis was used to achieve maximum alignment, followed by considerable filtering.[36] Later, a routine for noise reduction was devised based on correlation optimized warping of successive scans to correct for non-constant shifts in the fine structure throughout the spectrum.[17] A further impediment for accomplishing similar signal-to-noise ratios as with FT-IR spectrometers within reasonable time was the limited sweep velocity in the range of 100 cm^{-1} s^{-1} in early commercially available EC-QCLs. Using latest generation EC-QCLs, tuning rates of up to 25000 cm^{-1} s^{-1} (LaserTune, Block Engineering) and 5000 cm^{-1} s^{-1} (MIRcat-QT, Daylight Solutions) can been reached. Furthermore, scanning speeds of up to 600000 cm^{-1} s^{-1} have been published employing a resonantly driven micro-opto-electro-mechanical systems (MOEMS) grating.[37,38]

In this work, we present IR transmission measurements of proteins in aqueous solutions in the amide I and amide II region, employing a latest generation EC-QCL. A data-processing routine is presented for noise reduction, which discards occasional EC-QCL scans that are shifted in the wavenumber axis. The performance of the setup regarding SNR was compared to research-grade FT-IR spectrometers at equal acquisition times. The shape of the obtained IR spectra of proteins with different secondary structures were contrasted to FT-IR spectra and showed excellent comparability.

EXPERIMENTAL SECTION

Reagents and Samples. Sodium phosphate monobasic dihydrate p.a. (NaH$_2$PO$_4$•2H$_2$O) was purchased from Fluka (Buchs, Switzerland), sodium phosphate dibasic dihydrate (Na$_2$HPO$_4$•2H$_2$O) BioUltra, for molecular biology, and sodium hydroxide solution 50% in water, were obtained from Sigma-Aldrich (Steinheim, Germany). β-Lactoglobulin from bovine milk (≥85%), bovine serum albumin (≥98%) and lysozyme from chicken egg white (>90%) were obtained by Sigma-Aldrich (Steinheim, Germany) and used as purchased. Appropriate amount of lyophilized protein powder was dissolved in 16.0 mmol L^{-1} phosphate buffer pH 7.0. Ultrapure water (18 MΩ) was used for preparation of all solutions, obtained with a Milli-Q water purification system from Millipore (Bedford, USA).

FT-IR Measurements. FT-IR absorption measurements were performed using a Bruker Vertex 80v FT-IR spectrometer (Ettlingen, Germany) equipped with a liquid nitrogen cooled HgCdTe (mercury cadmium telluride) detector (D*= 4 × 10^{10} cm Hz$^{0.5}$ W^{-1} at 9.2 μm) and a Bruker Tensor 30 FT-IR spectrometer equipped with a DLaTGS (deuterated lanthanum α-alanine doped triglycine sulfate) detector (D*= 6 × 10^8 cm Hz$^{0.5}$ W^{-1} at 9.2 μm). The samples were placed between two CaF$_2$ windows separated by an 8 μm-thick spacer. During measurements, the spectrometer was flushed with dry air for at least 5 minutes prior to spectrum acquisition. Spectra were acquired with a spectral resolution of 2 cm^{-1} in double-sided acquisition mode. A total of 81 (Vertex operated at 80 kHz scanner velocity) and 21 (Tensor operated at 20 kHz scanner velocity) scans were averaged per spectrum (acquisition time: 53 s), which was calculated using a Blackman-Harris 3-term apodization function and a zero filling factor of 2. All spectra were acquired at 25 °C. Spectra were analyzed using the software package OPUS 7.2 (Bruker, Ettlingen, Germany). If necessary, absorption bands of water vapor in the atmosphere were subtracted.

Experimental Setup for QCL Measurements. The experimental setup is shown in Figure 1. For the measurements, a water-cooled external-cavity quantum cascade laser (Hedgehog, Daylight Solutions Inc., San Diego, USA) was used operating at a repetition rate of 100 kHz and a pulse width of 5000 ns, resulting in a duty cycle of 50%. The manufacturer states laser power variations of <3% RMS and an operating temperature range of 15-35 °C. The laser head temperature was set to 19 °C for all measurements. All spectra were recorded in the spectral tuning range between 1730–1470 cm^{-1}, covering the amide I and amide II region of proteins, at a scan speed of 1200 cm^{-1}s^{-1}. A mesh was employed to attenuate the laser intensity and a wedged sapphire window (2.5 mm thickness) was used to selectively reduce the laser intensity in the amide II region. The MIR light was focused on the detector element by a gold plated off-axis parabolic mirror with a focal length of 43 mm. A thermoelectrically-cooled MCT detector operating at -78 °C (PCI-10.6, Vigo Systems S.A., Poland) with a 0.5 × 0.5 mm element size and a detectivity of D* = 8 × 10^9 cm Hz$^{0.5}$ W^{-1} at 6 μm at 10 MHz was used as IR detector. To reduce the influence of

water vapor, the setup was placed in a housing of polyethylene foil and constantly flushed with dry air.

The measured signal was processed by a lock-in amplifier (Stanford Research Systems, CA, USA) and digitized by a NI DAQ 9239 24-bit ADC (National Instruments Corp., Austin, USA). Each single beam spectrum consisting of 6000 data points was recorded during the tuning time for one scan of approx. 250 µs. A total of 100 scans were recorded for background and sample single beam spectra at a total acquisition time of 53 s. The spectral resolution of the EC-QCL setup was determined by evaluation of the band width of water vapor spectra and comparison with FT-IR spectra acquired at different resolutions and was determined to be 0.2 cm^{-1} and 2 cm^{-1} for non-filtered and filtered spectra, respectively.

All measurements were carried out using a custom-built, temperature-controlled flow cell equipped with two MIR transparent CaF$_2$ windows and 31 µm-thick spacer, at 20 °C.

Deviations in the wavenumber scale of the recorded data introduced by the EC-QCL or data acquisition were corrected by calibration of the setup to the absorption lines of water vapor.

The laser was controlled by Daylight Solution driver software; data acquisition and temperature control was performed using a custom-made LabView-based GUI (National Instruments Corp., Austin, USA).
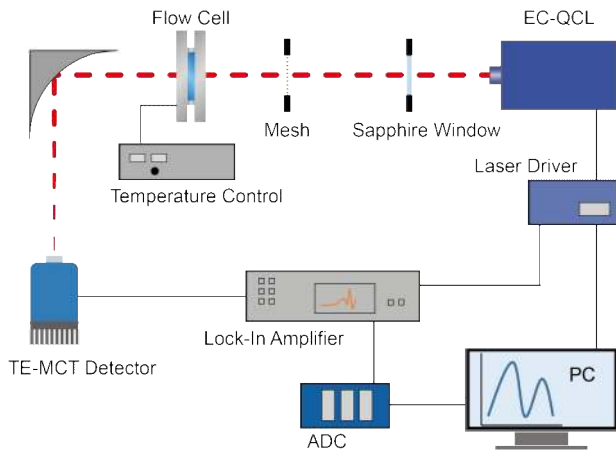

Figure 1. Schematic of the experimental QCL-based setup for mid-IR transmission measurements.

Processing of QCL Data. The performed preprocessing steps are schematically depicted in Figure 2. First, the measured data were treated by Savitzky-Golay smoothing to reduce instrumental noise. In order to sort out scans that are shifted more than 0.1 cm^{-1}, the similarity index of each scan was obtained by calculating the product of correlation coefficients between all individual scans. For a given scan x_t, the similarity index, ranging from 0 to 1, is calculated by the following expression

$$Similarity\ index = \prod_{i=1}^{100} |r(x_t, x_i)| \qquad (1)$$

in which r (x_t, x_i) is the correlation coefficient between the target scan and each of the remaining 99 scans. This approach has

been used to evaluate the similarity in chromatographic data.[39] Here, approx. 3% scans with a similarity index lower than 0.995 were sorted out employing this method.

A low-pass Fourier filter based on 4-term Blackman-Harris apodization (Fast Fourier Transformation-FFT) with a cutoff frequency of 150-200 was applied to single beam spectra I and I_0. The final absorption spectrum was obtained using

$$A = -\log\left(\frac{I}{I_0}\right) \qquad (2)$$

In order to quantitatively evaluate the comparability of the protein IR spectra acquired by EC-QCL and FT-IR spectroscopy by the degree of spectral overlap (s_{12}) between FT-IR (s_1) and EC-QCL (s_2), the following expression was employed:[40]

$$s_{12} = \frac{\|s_1^T s_2\|}{\|s_1\|\|s_2\|} \qquad (3)$$

This evaluation was performed for the presented absorbance spectra. The value of s_{12} ranges from 0 to 1, corresponding to no overlapping and complete overlapping, respectively.

Data processing and analysis was performed with in-house code developed in MatLab R2014b® (MathWorks, Inc., Natick, MA, 2014).
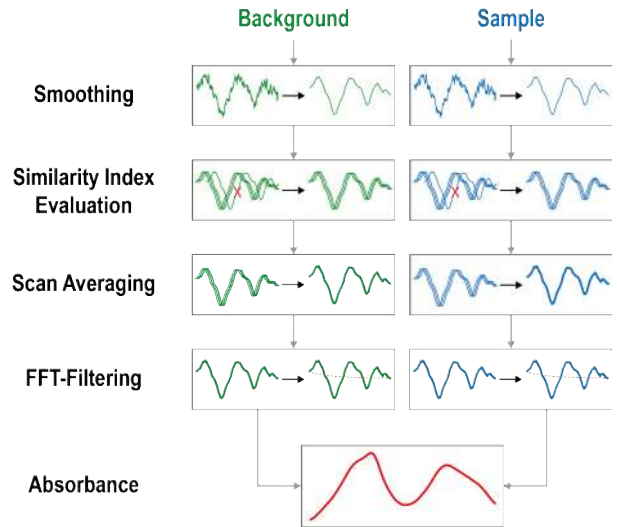

Figure 2. Sequence of processing steps for EC-QCL IR transmission spectra.

RESULTS AND DISCUSSION

Mid-IR Spectra recorded with the EC-QCL Setup. IR spectra of proteins at different concentrations were recorded by using the custom-made laser-based IR transmission setup employing a transmission path length of 31 µm (Fig. 1). The broad tuning range of the applied EC-QCL allows to record spectra across the amide I and amide II range, thus enabling
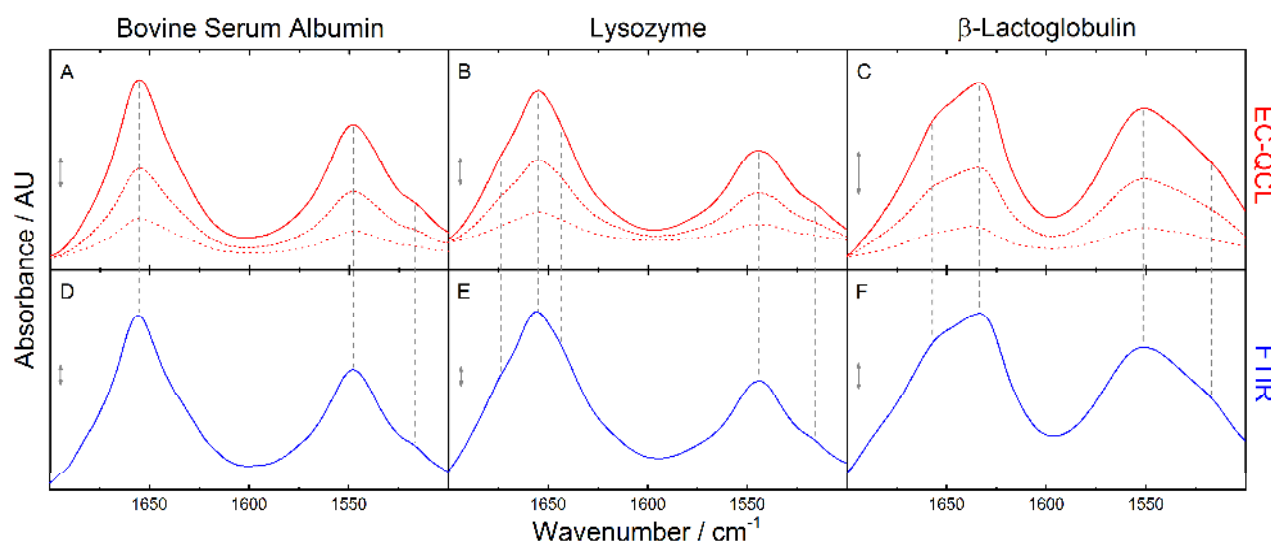
Figure 3. IR absorbance spectra of 5 (red solid line), 2.5 (red dashed line) and 1 mg mL^{-1} (red dotted line) protein solutions acquired by the EC-QCL setup (A-C) and 20 mg mL^{-1} (blue solid line) protein solutions acquired by FT-IR spectroscopy (D-F). Grey dashed lines highlight the high congruence of the spectral features between the IR spectra acquired by EC-QCL and FT-IR spectroscopy. Grey double-headed arrows indicate the absorbance of 5 mAU.

quantitative as well as qualitative evaluation of the protein spectra. The investigated model proteins exhibit characteristic spectral features of different secondary structures. (Fig. 3A-C). Bovine serum albumin (BSA) is a well-studied protein consisting primarily of α-helical structures,[41,42] and shows the α-helix characteristic band at 1656 cm^{-1} in the amide I region,[1] as well as a narrow band at approx. 1545 cm^{-1} in the amide II region.[9,43] β-lactoglobulin (β-LG) is mainly composed of β-sheet secondary structure and displays a distinctive IR band maximum at 1633 cm^{-1} and a shoulder at 1680 cm^{-1} in the amide I region,[44] and a broad band at approx. 1550 cm^{-1} in the amide II region.[9] Lysozyme (Lys) contains both α-helices and β-sheets resulting in a band maximum at 1656 cm^{-1} with shoulders at ~1640 cm^{-1} and ~1675 cm^{-1} in the amide I region and a narrow band at 1545 cm^{-1} in the amide II region.[6,41] Characteristic spectral features of the individual secondary structures could be identified at protein concentrations as low as 1 mg mL^{-1} in aqueous solution. For reference, FT-IR spectra of the protein solutions were recorded (Fig. 3D-F). Comparison analysis between spectra reveals excellent agreement of the protein spectra recorded by using the EC-QCL-based setup with the spectra.

Band areas of the amide I and amide II regions were evaluated for the protein solutions in six concentrations. Calibration curves in Figure S1 show that the data fitted well to a linear regression line (r^2 >0.99), with linearity down to a concentration of 0.5 mg mL^{-1}. This demonstrated validity of the Lambert Beer law is significant for prospective applications of this setup for quantitative analysis.

Optimization of Laser Power and Transmission Path Length. Prior to incorporating the employed, latest generation EC-QCL light source into the transmission setup, its emission characteristics were thoroughly examined. The maximum power is emitted at approx. 1600 cm^{-1} and decreases in both spectral directions, as depicted in Figure S2A. Water in the transmission cell absorbs a large part of the irradiated light

around the center of the HOH-bending band at 1645 cm^{-1}. Consequently, in this spectral region (i.e. amide I region) the energy reaching the detector is significantly lower than in regions without water absorption (i.e. amide II region). This high difference between maximum and minimum intensity at the detector exceeds its dynamic range. Figure S2B shows the recorded single beam spectrum at a path length of 31 µm at the highest laser current setting, resulting in the absorbance spectrum shown in Figure S2C. The high intensity in the amide II region leads to detector saturation. For EC-QCLs, the emission power cannot simply be diminished by reducing the laser current, as then also the wavelength emission range is restricted. Optimization of the laser intensity with the sapphire window and mesh is a tradeoff between accomplishable transmission path length and accessible spectral range. In the present situation, selective attenuation in the amide II region is desired in order to match the strong solvent absorption in the amide I region. For this purpose, a wedged sapphire window was employed that acts as a short-wave pass filter with a cut-off at approx. 1650 cm^{-1}. A mesh was used to further reduce the laser intensity across the entire spectral region. By employing these measures, single beam spectra could be achieved that are in accordance with the dynamic range of the detector (Figure S2B) and absorbance spectra can be obtained across the entire amide I and amide II regions (Figure S2C).

Laser Performance and Data Processing. The laser performance of the latest generation EC-QCL employed in the herein presented setup was compared to emission characteristics of a first generation EC-QCL that was used in an earlier setup.[17] A particular focus was on the reproducibility of wavelength tuning. In first generation EC-QCLs, mechanical imperfections and triggering issues lead to spectral mismatch in the fine structure of consecutive scans. The introduced deviations seemed small in the single beam spectra but prevented scan accumulation and introduced considerable noise in the absorbance spectrum. For comparison of the noise levels, 100% lines of water
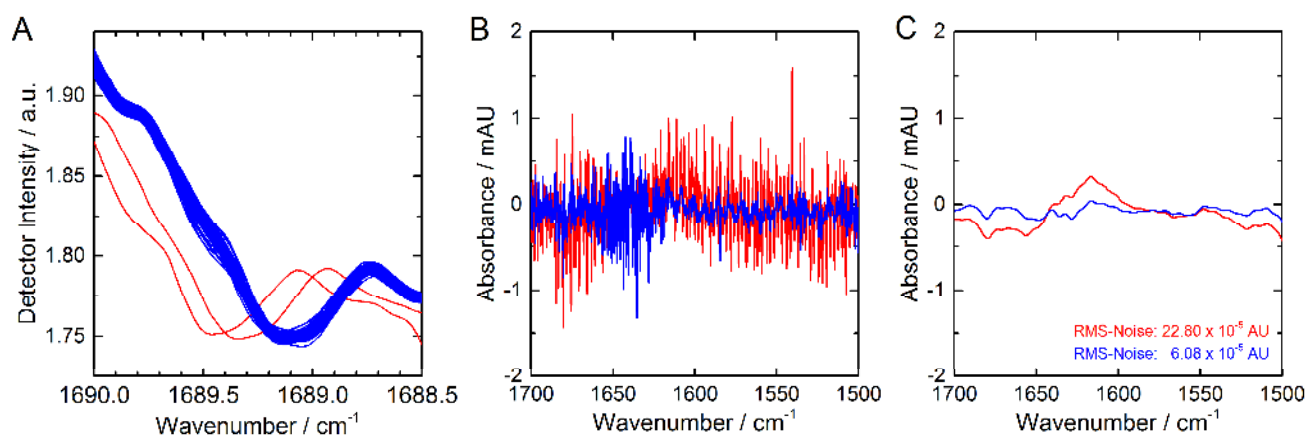
Figure 4. (A) Close-up of 100 single beam scans recorded by the EC-QCL setup. The red spectra were rejected during data processing. (B) Unfiltered 100% lines of water (blue) with and (red) without similarity index evaluation. (C) Filtered 100% lines of water (blue) with and (red) without similarity index evaluation.

were employed that are obtained by calculating the absorbance spectra of two subsequent single beam spectra of the same sample under the same conditions. Under ideal conditions, the result is a flat line at 100% transmittance, corresponding to zero absorbance.[45] The RMS noise was calculated between 1700-1600 cm^{-1}. Figure 4A shows a close-up of 100 single beam scans, acquired with the presented EC-QCL setup. Most of the scans are highly overlapping, whereas two are clearly separated and shifted by approx. 0.5 cm^{-1}. Comparison with the single beam scans emitted by a first generation EC-QCL reveals that the reproducibility of the wavelength tuning is substantially more precise when using a latest generation EC-QCL. This may be the result of optimized motion mechanics and triggering routines of the external cavity. As depicted in Figure S3A, the individual scans of the first generation laser were randomly distributed across a wavenumber range of 0.5 cm^{-1}. This shift was successfully corrected by COW, a rubberband type alignment approach, which allowed to reduce the noise level of the absorbance spectra by a factor of approx. 8 and RMS-noise of 26.4 x 10^{-5} AU could be achieved (see Figure S3D).

Compared to that, with the newly developed setup even lower RMS noise (22.8 x 10^{-5} AU) could be achieved without any further data processing (see Figure 4). By application of the COW routine, this value could be lowered by 40% (see Figure S4D). However, better noise values were expected for this setup configuration employing modulated laser emission and lock-in amplification. For this reason, a new approach for data processing was conceived, as outlined in Figure 2. It is based on calculation of the similarity index, which is the product of the correlation coefficients between all individual spectra. For every spectrum, a value is obtained between 1 and 0, corresponding to high and low similarity, respectively. This evaluation step is performed for the background and sample single channel spectra prior to scan averaging. Figure S5A shows a representative plot of the similarity index evaluation of 100 scans. Obviously, two scans considerably deviate from the remaining ones, indicated by a low similarity index (marked red in Figure S5A). Prior to further processing, deviating scans with a similarity index lower than 0.995 are removed. After scan averaging, minor Fourier filtering is applied, with a cutoff frequency of 200 Hz.

Finally, the similarity index was also employed for the quantification of the initially mentioned tuning precision of the laser

emission wavelength, and comparison of the two laser generations. For the first generation laser, a similarity index of 0.510 with pronounced scattering was reached on average for 100 scans. By application of the COW alignment routine, this value could be increased to 0.977. In contrast, the similarity index obtained for the latest generation laser is above 0.995 even before data processing.

Comparison of mid-IR Spectra recorded with the EC-QCL Setup and FT-IR Spectroscopy. FT-IR measurements of protein solutions were performed in order to compare results with the spectra recorded with the presented EC-QCL setup. Figure 3D-F show the IR spectra of 20 mg mL^{-1} protein solutions acquired at a path length of 8 μm. Evaluation of band positions and shape of the IR absorption spectra illustrates the high comparability between QCL-IR spectra and conventional FT-IR spectroscopy. For quantification of the congruence between the (normalized) data sets, the degree of spectral overlap was computed. Employing eq 3, the s_{12} values obtained for BSA, β-LG and Lys were 0.99175, 0.99444 and 0.99585, respectively, indicating excellent comparability between QCL-IR and FT-IR spectra.
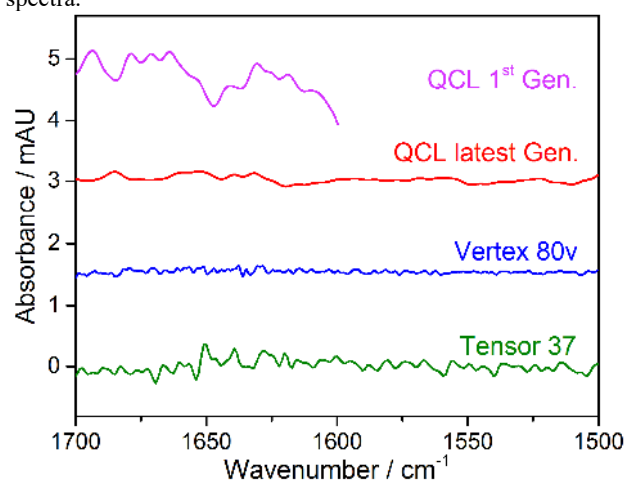

Figure 5. Comparison of recorded 100% lines of water obtained by two different types of EC-QCL setups and FT-IR spectrometers.

Table 1: Characteristic parameters and relevant results for comparing the performance of EC-QCL based IR transmission setups and conventional FT-IR spectroscopy.

	Meas. time [s] / scans	RMS-Noise 10^{-5} [AU]	Path length [μm]	SNR*	Spectral range [cm^{-1}]	Detector type / temp. [°C] / cooling
QCL setup 1st gen.	250 / 100	37	38	515	1700-1600	MCT / -60 / TE
QCL setup latest gen.	53 / 100	6.2	31	2425	1700-1500	MCT / -78 / TE
High-end FT-IR	53 / 81	2.7	8	1481	4000-600	MCT / -196 / LN$_2$
Routine FT-IR	53 / 21	12.1	8	329	4000-600	DLaTGS / 25 / ---

* Evaluated for 20 mg mL^{-1} protein solution.

Furthermore, the noise performance of the developed laser-based setup was evaluated and compared to a custom-built IR transmission setup employing a first generation EC-QCL[17] as well as with commercially available FT-IR spectrometers. Characteristic parameters and evaluated results are summarized in Table 1. For evaluation of the noise performance, the RMS (root-mean-square) noise of the 100% lines of water in the region of 1700-1600 cm^{-1} were calculated. When comparing the two EC-QCL based setups, with the latest generation laser, lower noise levels by a factor of ~6 were achieved employing approx. one fifth of the measurement time. Faster acquisition times for recording the same number of scans across doubled wavenumber range could be achieved due to the much higher sweep rates of the employed EC-QCL. Low noise levels were obtained because of the increased wavenumber reproducibility of consecutive scans in the initially recorded raw spectra and the developed processing routine to eliminate single deviating scans, as outlined in detail above. The slightly lower achievable path length with the latest generation EC-QCL setup results from the tradeoff between the path length and the dynamic range of the detector at the wide spectral emission range. Finally, with the IR transmission setup presented here, a SNR better by a factor of ~5 could be accomplished than with the first generation EC-QCL setup.

The newly developed EC-QCL based IR transmission setup was also benchmarked against FT-IR spectroscopy. For this comparison, a high-end FT-IR spectrometer with a fast interferometer and a liquid nitrogen cooled MCT detector as well as a routine FT-IR instrument with a pyroelectric detector were used as a reference. The acquisition times of water 100% lines were equal to the ones used for the EC-QCL IR transmission setup. For FT-IR measurements, a path length of 8 μm was employed. The noise level obtained with the high-end FT-IR spectrometer was approx. 2.3 times lower than with the laser-based setup. For a complete assessment of the noise level of a measurement, all contributors need to be considered. Referring to the light source, the noise level introduced by low intensity thermal light sources in FT-IR spectrometers can usually be neglected. High intensity laser sources, however, contribute to the overall measurement noise, particularly when operated in pulsed mode due to pulse-to-pulse intensity fluctuations.[33,36,46] Figure S6 shows Allan deviation plots recorded with the presented setup, indicating that the noise is limited by the EC-QCL light source. Regarding the detector, the detectivity of the LN$_2$ cooled MCT detector employed in the FT-IR spectrometer is 5 times higher than the Peltier-cooled MCT detector applied in the EC-QCL setup. Due to the difference of the employed detectors, the same data acquisition time as well as the same spectral resolution were chosen

for the measurements of the 100% lines in order to compare the performance of the instrument configurations. Although the measured noise levels were lower with the high-end FTIR spectrometer, due to the higher applicable path length, with the laser-based setup a SNR better by a factor of approx. 2 can be reached compared to the high-end FT-IR spectrometer. Comparison with the routine FT-IR spectrometer reveals a SNR better by a factor of approx. 7 for the EC-QCL setup. Finally, for FT-IR spectroscopy the advantage of total spectral coverage of the mid-IR region should be noted.

CONCLUSIONS AND OUTLOOK

An IR transmission setup based on a latest generation EC-QCL was presented for protein analysis in the amide I and amide II regions. Characteristic spectral features of multiple proteins with different secondary structure were successfully measured at concentrations as low as 1 mg mL^{-1}. Usage of a latest generation EC-QCL facilitated high wavelength repeatability between scans and fast sweep rates. Application of a data processing routine accomplished SNR values higher than reached for FT-IR spectroscopy, the gold standard for broadband IR transmission spectroscopy, at similar measurement times. In this context, the presented work marks a further example of QCL-based setups performing beyond FT-IR instruments. In the field of IR imaging even higher gains in the SNR (>100) at similar measurement times could be obtained by application of QCLs. Here, another feature of EC-QCLs is utilized, which is the possibility to sequentially measure at individual wavenumbers without the need of recording the entire spectrum. With this concept of discrete frequency imaging, where imaging data is measured at a reduced set of wavenumbers that provide the relevant information, the measurement time could be significantly lowered.[47-50]

For the herein presented EC-QCL based IR transmission measurements, further noise reduction employing the laser-based setup is envisioned by implementing a balanced detection scheme. Even though there is the limitation of the spectral coverage compared to FT-IR spectroscopy due to the restricted emission range of EC-QCLs, a pronounced advantage of the presented setup is the accessibility of the amide I region at robust and conveniently manageable optical paths. The large optical paths can be used for directly measuring IR absorbance spectra of water-based solutions such as body fluids (e.g. blood, serum, mother's milk), foodstuff (e.g. commercial milk) or process analytical solutions. These liquids feature a complex matrix composition with increased viscosity and H-D exchange for D$_2$O based IR analysis is not possible or not achievable in a

timely manner to provide the results in an acceptable time-frame. Compared to the earlier laser-based IR transmission setup, the expanded spectral coverage, including the most prominent protein IR bands, provides advantages for qualitative and quantitative protein studies. In the future, the presented setup will be employed to investigate dynamic secondary structure changes and chemometrics-based protein quantification in complex matrices.

ASSOCIATED CONTENT

Supporting Information

The Supporting Information is available free of charge on the ACS Publications website at DOI: 10.1021/acs.analchem.0000000.
Figure S1. Calibration curves for proteins. Figure S2. Laser emission curve, single beam spectra and absorbance spectra with and without attenuation. Figure S3. Single beam and absorbance spectra of a first generation EC-QCL before and after alignment by COW. Figure S4. Single beam and absorbance spectra of a latest generation EC-QCL before and after alignment by COW. Figure S5. Similarity index evaluation. Figure S6. Allan deviation plot of detector and laser.

AUTHOR INFORMATION

Corresponding Author

*E-mail: bernhard.lendl@tuwien.ac.at.

Author Contributions

‡These authors contributed equally to this work

Notes

The authors declare no competing financial interest.

ACKNOWLEDGMENTS

REFERENCES

(1)   Barth, A. *Biochim. Biophys. Acta, Bioenerg.* **2007**, *1767*, 1073-1101.
(2)   Gerwert, K.; Freier, E.; Wolf, S. *Biochim. Biophys. Acta, Bioenerg.* **2014**, *1837*, 606-613.
(3)   Kotting, C.; Gerwert, K. *ChemPhysChem* **2005**, *6*, 881-888.
(4)   Bal Ram, S. In *Infrared Analysis of Peptides and Proteins*; American Chemical Society, 1999, pp 2-37.
(5)   Fabian, H.; Mäntele, W. In *Handbook of Vibrational Spectroscopy*; John Wiley & Sons, Ltd: Hoboken, NJ, USA, 2006.
(6)   van de Weert, M.; Haris, P. I.; Hennink, W. E.; Crommelin, D. J. A. *Anal. Biochem.* **2001**, *297*, 160-169.
(7)   Brian, M. M.; Jennifer, D.; Antonio; Mark, C. M.; Wasfi, A.-A. *Curr. Pharm. Biotechnol.* **2014**, *15*, 880-889.
(8)   Alcaráz, M. R.; Schwaighofer, A.; Goicoechea, H.; Lendl, B. *Spectrochim. Acta, Part A* **2017**, *185*, 304-309.
(9)   Dousseau, F.; Pezolet, M. *Biochemistry* **1990**, *29*, 8771-8779.
(10)   Navea, S.; Tauler, R.; Goormaghtigh, E.; de Juan, A. *Proteins* **2006**, *63*, 527-541.
(11)   Yang, H.; Yang, S.; Kong, J.; Dong, A.; Yu, S. *Nat. Protoc.* **2015**, *10*, 382-396.
(12)   Weida, M. J.; Yee, B. *Proc. Soc. Photo-Opt. Instrum. Eng.* **2011**, *7902*, 79021C.
(13)   Kosterev, A.; Wysocki, G.; Bakhirkin, Y.; So, S.; Lewicki, R.; Fraser, M.; Tittel, F.; Curl, R. F. *Appl. Phys. B: Lasers Opt.* **2008**, *90*, 165-176.
(14)   Brandstetter, M.; Genner, A.; Anic, K.; Lendl, B. *Analyst* **2010**, *135*, 3260-3265.
(15)   Brandstetter, M.; Volgger, L.; Genner, A.; Jungbauer, C.; Lendl, B. *Appl. Phys. B: Lasers Opt.* **2013**, *110*, 233-239.
(16)   Brandstetter, M.; Sumalowitsch, T.; Genner, A.; Posch, A. E.; Herwig, C.; Drolz, A.; Fuhrmann, V.; Perkmann, T.; Lendl, B. *Analyst* **2013**, *138*, 4022-4028.
(17)   Alcaráz, M. R.; Schwaighofer, A.; Kristament, C.; Ramer, G.; Brandstetter, M.; Goicoechea, H.; Lendl, B. *Anal. Chem.* **2015**, *87*, 6980-6987.
(18)   Alcaráz, M. R.; Schwaighofer, A.; Goicoechea, H.; Lendl, B. *Anal. Bioanal. Chem.* **2016**, *408*, 3933-3941.
(19)   Schwaighofer, A.; Alcaraz, M. R.; Araman, C.; Goicoechea, H.; Lendl, B. *Sci. Rep.* **2016**, *6*, 33556.
(20)   Kuligowski, J.; Schwaighofer, A.; Alcaráz, M. R.; Quintás, G.; Mayer, H.; Vento, M.; Lendl, B. *Anal. Chim. Acta* **2017**, *963*, 99-105.
(21)   Schwaighofer, A.; Kuligowski, J.; Quintás, G.; Mayer, H. K.; Lendl, B. *Food Chem.* **2018**, *252*, 22-27.
(22)   Schwaighofer, A.; Alcaráz, M. R.; Kuligowski, J.; Lendl, B. *Biomed. Spectrosc. Imaging* **2018**, *7*, 35-45.
(23)   Schultz, B. J.; Mohrmann, H.; Lorenz-Fonfria, V. A.; Heberle, J. *Spectrochim. Acta, Part A* **2018**, *188*, 666-674.
(24)   Lórenz-Fonfría, V. A.; Schultz, B.-J.; Resler, T.; Schlesinger, R.; Bamann, C.; Bamberg, E.; Heberle, J. *J. Am. Chem. Soc.* **2015**, *137*, 1850-1861.
(25)   Resler, T.; Schultz, B.-J.; Lórenz-Fonfría, Víctor A.; Schlesinger, R.; Heberle, J. *Biophys. J.* **2015**, *109*, 287-297.
(26)   López-Lorente, Á. I.; Wang, P.; Sieger, M.; Vargas Catalan, E.; Karlsson, M.; Nikolajeff, F.; Österlund, L.; Mizaikoff, B. *Phys. Status Solidi A* **2016**, *213*, 2117–2123.
(27)   Haas, J.; Stach, R.; Sieger, M.; Gashi, Z.; Godejohann, M.; Mizaikoff, B. *Anal. Methods* **2016**, *8*, 6602-6606
(28)   Lambrecht, A.; Pfeifer, M.; Konz, W.; Herbst, J.; Axtmann, F. *Analyst* **2014**, *139*, 2070-2078.
(29)   Kristament, C.; Schwaighofer, A.; Montemurro, M.; Lendl, B. *Proceedings of SPIE-The International Society for Optical Engineering* **2018**, *10490*, 104900M.
(30)   Lüdeke, S.; Pfeifer, M.; Fischer, P. *J. Am. Chem. Soc.* **2011**, *133*, 5704-5707.
(31)   Rüther, A.; Pfeifer, M.; Lórenz-Fonfría, V. A.; Lüdeke, S. *J. Phys. Chem. B* **2014**, *118*, 3941-3949.
(32)   Rüther, A.; Pfeifer, M.; Lórenz-Fonfría, V. A.; Lüdeke, S. *Chirality* **2014**, *26*, 490-496.
(33)   Hayden, J.; Hugger, S.; Fuchs, F.; Lendl, B. *Appl. Phys. B: Lasers Opt.* **2018**, *124*, 29.
(34)   Schwaighofer, A.; Brandstetter, M.; Lendl, B. *Chem. Soc. Rev.* **2017**, *46*, 5903-5924.
(35)   Siebert, F.; Hildebrandt, P.; Wiley-VCH Verlag GmbH & Co. KGaA: Weinheim, 2008.
(36)   Brandstetter, M.; Koch, C.; Genner, A.; Lendl, B. *Proc. SPIE* **2014**, *8993*, 89931u.

(37)   Butschek, L.; Hugger, S.; Jarvis, J.; Haertelt, M.; Merten, A.; Schwarzenberg, M.; Grahmann, J.; Stothard, D. M.; Warden, M.; Carson, C.; Macarthur, J.; Fuchs, F.; Ostendorf, R.; Wagner, J.; SPIE, 2017, p 10.

(38)   Butschek, L.; Hugger, S.; Jarvis, J.; Haertelt, M.; Merten, A.; Grahmann, J.; Boskovic, D.; Fuchs, F.; Ostendorf, R.; Schilling, C.; Rattunde, M.; Wagner, J. In *SPIE OPTO*; SPIE, 2017, p 11.

(39)   Skov, T.; van den Berg, F.; Tomasi, G.; Bro, R. *J. Chemom.* **2006**, *20*, 484-497.

(40)   Culzoni, M. J.; Goicoechea, H. C.; Ibañez, G. A.; Lozano, V. A.; Marsili, N. R.; Olivieri, A. C.; Pagani, A. P. *Anal. Chim. Acta* **2008**, *614*, 46-57.

(41)   Levitt, M.; Greer, J. *J. Mol. Biol.* **1977**, *114*, 181-239.

(42)   Grdadolink, J.; Marechal, Y. *Biopolymers* **2001**, *62*, 40-53.

(43)   Lin, S. Y.; Wu, C. W.; Liang, R. C. *Eur. J. Clin. Chem. Clin. Biochem.* **1995**, *33*, 255-261.

(44)   Monaco, H. L.; Zanotti, G.; Spadon, P.; Bolognesi, M.; Sawyer, L.; Eliopoulos, E. E. *J. Mol. Biol.* **1987**, *197*, 695-706.

(45)   Brandstetter, M.; Lendl, B. *Sens. Actuators, B* **2012**, *170*, 189-195.

(46)   Childs, D. T. D.; Hogg, R. A.; Revin, D. G.; Rehman, I. U.; Cockburn, J. W.; Matcher, S. J. *Appl. Spectrosc. Rev.* **2015**, *50*, 822-839.

(47)   Yeh, K.; Kenkel, S.; Liu, J.-N.; Bhargava, R. *Anal. Chem.* **2015**, *87*, 485-493.

(48)   Hughes, C.; Clemens, G.; Bird, B.; Dawson, T.; Ashton, K. M.; Jenkinson, M. D.; Brodbelt, A.; Weida, M.; Fotheringham, E.; Barre, M.; Rowlette, J.; Baker, M. J. *Sci. Rep.* **2016**, *6*, 20173

(49)   Kole, M. R.; Reddy, R. K.; Schulmerich, M. V.; Gelber, M. K.; Bhargava, R. *Anal. Chem.* **2012**, *84*, 10366-10372.

(50)   Pilling, M. J.; Henderson, A.; Gardner, P. *Anal. Chem.* **2017**, *89*, 7348-7355.

For Table of Contents Only